JOURNAL OF SOLID STATE CHEMISTRY **122,** 186–194 (1996)
ARTICLE NO. 0100

Phenomenology of Polymorphism, III: *p,T* Diagram and Stability of Piracetam Polymorphs

R. Céolin,*,§,[1] V. Agafonov,* D. Louër,† V. A. Dzyabchenko,‡ S. Toscani,§ and J. M. Cense**

*Laboratoire de Chimie Physique, Faculté de Pharmacie, 31, avenue Monge, 37200 Tours Cedex, France; †Laboratoire de Cristallochimie, URA CNRS 1495, Université de Rennes I, avenue du Général Leclerc, 35042 Rennes Cedex, France; ‡Karpov Institute of Physical Chemistry, ul. Obukha 10, Moscow 107120, Russia; §Laboratoire de Chimie Physique et Chimie Minérale, Faculté de Pharmacie, 4, avenue de l'Observatoire, 75270 Paris Cedex 06, France; and **U.R. Modélisation Appliquée à la Chimie et aux Procédés, ENSCP, 11, rue P. et M. Curie, 75231 Paris Cedex 05, France

Received July 28, 1995; in revised form November 22, 1995; accepted December 19, 1995

The nootropic drug Piracetam is known to crystallize in three phases. In order to obtain their stability hierarchy from sublimation pressure inequalities, the drawing of a topological *p,T* diagram was attempted. For such a purpose and also for quality control, crystallographic and thermodynamic data were required. Powder X-ray diffractometry (XRD) and differential scanning calorimetry (DSC) were used. Molecular energy calculations were performed. Phase I melts at 426 K ($\Delta_{fus}H(I) = +180\ J \cdot g^{-1}$). Phase II transforms into Phase I at 399 K ($\Delta_{(II\rightarrow I)}H = +24\ J \cdot g^{-1}$). Phase III transforms into phase I at 392 K ($\Delta_{(III\rightarrow I)}H = +28\ J \cdot g^{-1}$) or melts at 412 K ($\Delta_{fus}H(III) = +210\ J \cdot g^{-1}$). The *p,T* diagram shows that phase I is stable at higher temperature and phase II at lower temperature, like phase III, which is stable under high pressure. At room temperature, phase II is the more stable form, and phase I the less stable one. This agrees with the spontaneous I → II transformation observed at 298 K within a few hours, and with lattice energies, calculated previously. Molecular energy calculations and crystal structure comparison show how intermolecular hydrogen bonds and H-bonded dimers, in phases II and III, may stabilize conformations higher in energy than those of the isolated molecule and of phase I.

I. INTRODUCTION

Since polymorphism is known to be concerned with drugs (1), a stability hierarchy has to be established among the different crystalline varieties which can occur or interconvert when preparing, purifying, or storing a drug.

This hierarchy is deduced from the inequalities between the Gibbs free energies of the polymorphs at fixed values of temperature and pressure. It can also be determined from the *p,T* state diagram by comparing their vapor pressures, following Ostwald (2): the lower the sublimation pressure, the stabler the phase. In previous papers (3–5), it has been shown how topological *p,T* diagrams may be obtained from enthalpic and crystallographic studies, and how they may account for the inequalities of the vapor pressures of the polymorphs at any temperature. In this paper, Piracetam polymorphism is investigated.

Three crystalline phases of the nootropic drug Piracetam (6), (2-oxo-1-pyrrolidinyl)acetamide ($C_6H_{10}N_2O_2$, M = 142.2), have been identified first by Pavlova (7), by means of IR spectrometry and powder XRD. They may be obtained by crystallization from solutions in various solvents, as indicated by Pavlova *et al.* (8), who also pointed out that (a) their melting points range from 418 to 426 K, (b) phase I_p and phase II_p transform in the range 403 to 413 K, (c) phase III_p melts without transformation, and (d) humidity slowly transforms phase III_p into phase I_p at room temperature. DSC reveals (9) that phase III_p melts at 425 K, and that phases I_p and II_p both transform into phase III_p before melting (index p refers to Pavlova's nomenclature, that does not agree with the convention according to which polymorphs are identified by increasing roman numbers as their melting points decrease).

The crystal structures of these phases are known. Two of them, determined from single crystal XRD at room temperature, are monoclinic (6, 10, 11) and triclinic (10), respectively. The melting of this monoclinic phase is observed (10) at 411 K. The structure of the third phase, which is also monoclinic, has just been determined (12) by combining high resolution powder XRD with the atom–atom potential (AAP) method. From XRD profiles in Ref. (7), monoclinic and triclinic phases of Ref. (10) may correspond to phases II_p and I_p, respectively.

In this paper, the polymorphs are identified with the same symbols as in Ref. (13): the monoclinic and triclinic phases (10) correspond to phases III and II, respectively, and the third phase (12) to phase I (Table 1).

Interconversions and stabilities of these polymorphs

[1] To whom correspondence should be addressed.

0022-4596/96 $18.00

TABLE 1
Crystallographic Data for Phases I, II, and III at Room Temperature and Stability Hierarchy as a Function of Temperature

Phase	I	II	III
Ref.	(12)	(10)	(10)
Lattice	Monoclinic	Triclinic	Monoclinic
Space group	$P2_1/n$	$P\bar{1}$	$P2_1/n$
a (Å)	6.747	6.403	6.525
b (Å)	13.418	6.618	6.440
c (Å)	8.090	8.556	16.463
α (°)	90.0	79.85	90.0
β (°)	99.01	102.39	92.19
γ (°)	90.0	91.09	90.0
V_{cell} (Å^3)	723.36	348.51	691.29
Z	4	2	4
$V_{molecule}$ (Å^3)	180.84	174.26	172.82
d_{calc}(g · cm^{-3})	1.306	1.355	1.366
d_{obs}(g · cm^{-3}) (13)	1.304	1.351	1.371
T range (K)	<392	392–399	399–426
Vapor pressure[a]	pII < pIII < pI	pII < pI < pIII	pI < pII < pIII
Stability hierarchy[b]	SII > SIII > SI	SII > SI > SIII	SI > SII > SIII

Note. The slopes of the i–j transition curves have been calculated from the molecular volume values given in the table.
[a] p denotes vapor pressure.
[b] S denotes stability.

have been reexamined (13), and three other phases with high metastability degrees have been evidenced. Melting points of phases I, II, and III have been found at 426, 415.5, and 415 K, respectively. The transition II → I was observed at 348 K. From the energy vs temperature diagram, it was inferred that phase III is the more stable phase at 298 K, that phase I is the less stable one, and that phase III endothermally transforms into I at temperature higher than 348 K.

II. EXPERIMENTAL

II.A. Preparation and Characterization of Polymorphs

II.A.1. Preparation. Commercial samples of Piracetam powder were obtained from Isochem, France.

Phases III and II were grown by slowly evaporating at room temperature Piracetam solutions in methanol and in an isobutanol–water 95:5 (v:v) mixture, respectively.

Phase I was prepared by quenching phase II from 426 K down to room temperature.

II.A.2. Crystallographic data. Powder XRD spectra were obtained with an ENRAF-NONIUS FR553 (The Netherlands) camera (λCu$K\alpha$1 = 1.54059 Å); the spectrum of phase I was also recorded with a high resolution D500 SIEMENS (Germany) diffractometer with monochromatic X-rays (λCu$K\alpha$1 = 1.54059 Å). All spectra were indexed by using the LAZY program (Fig. 1). The observed interplanar distances agreed with those calculated, and no unindexed reflection was observed. For phase I, no extra diffraction peak was observed when the samples were analyzed as soon as quenched. Since experiments, described below, had shown that phase I does not persist at room temperature and transforms into phase II, thermodynamic studies on phase I have been carried out immediately after quenching.

II.A.3. Thermodynamic data. DSC experiments have been performed at 2, 5, and 10 K min^{-1} heating rates with the heating cell FP85 of a METTLER FP800 (Switzerland) system, and with the DSC cell of a T.A. Instruments (U.S.A.) thermal analyzer. Indium has been used as a standard for temperature and enthalpy calibration.

Samples of 5–10 mg, some being made up of a few single crystals, were weighed with a 0.01-mg-sensitive SETARAM γ21 (France) microbalance and sealed under air in aluminium pans. The enthalpy change values (ΔH) reported below result from the averaging of at least 5 runs. The transition temperatures are taken at the onset of the peaks with an accuracy of ±1 K. Accuracy on fusion enthalpies was 5%, and that on transition enthalpies could reach 10%.

Phase I melts at 426 K with a $\Delta_{fus}H$(I) value of +180 J · g^{-1} in close agreement with $\Delta_{fus}H$(I) = +180.7 J · g^{-1} (T_{fus}(I) = 426 K) of Ref. (13). Phase II transforms into phase I at 399 K (Fig. 2A) with $\Delta_{(II\to I)}H$ = +24 J · g^{-1} [from Ref. (13), $\Delta_{(II\to I)}H$ = +21 J · g^{-1} at $T_{II\to I}$ = 348 K (thermomicroscopy) or ca. 377 K (DSC)]. Phase III trans-

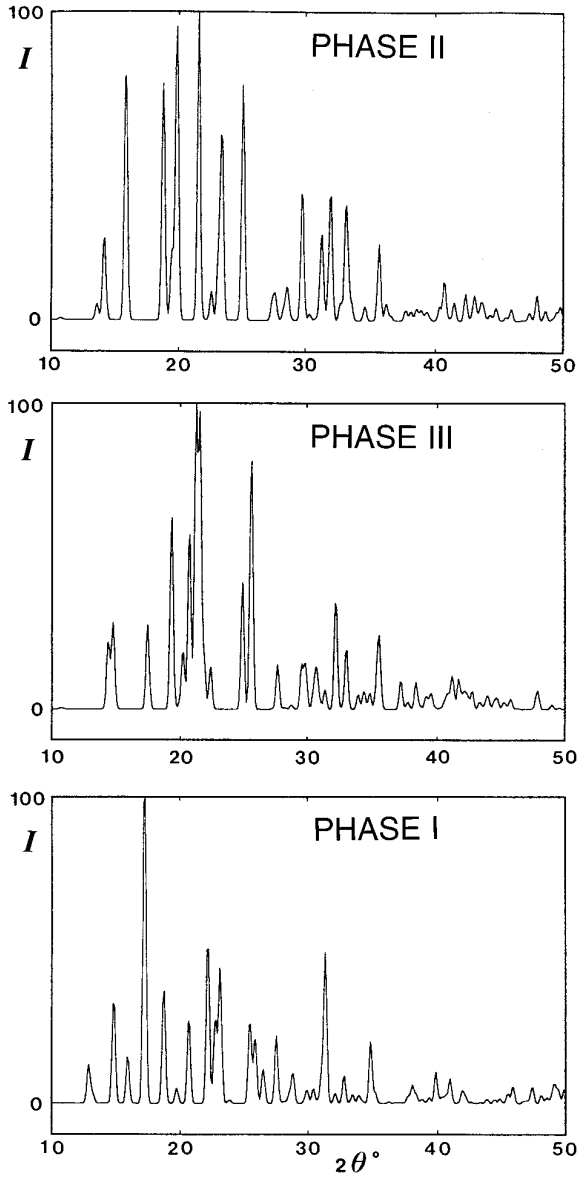

FIG. 1. X-ray powder diffraction profiles (intensity I (arbitrary units) vs $2\theta^{\circ}$).

forms into phase I at 392 K (Fig. 2C) with $\Delta_{(III\rightarrow I)}H = +28$ $J \cdot g^{-1}$ [from Ref. (13), $\Delta_{(III\rightarrow I)}H = +26.7$ $J \cdot g^{-1}$, $T_{III\rightarrow I}$ at ca. 390 K (DSC)]. The solid–solid transformations were identified by XRD of samples quenched as soon as the related endotherms were recorded.

It was observed that (i) some samples of phase III did not transform into phase I but melted at 412 K (Fig. 2D) with $\Delta_{fus}H(III) = +210$ $J \cdot g^{-1}$ [from Ref. (13), $T_{fus}(III) =$ 413 K, $\Delta_{fus}H(III) = 206$ $J \cdot g^{-1}$], and (ii) DSC curves of both phase II and III samples sometimes exhibited a weak endothermal effect (onset at ca. 415 K) after the peak of transition was recorded (arrows on Figs. 2B and 2C).

II.B. Isothermal Transformation of Phase I into Phase II

Data acquisition for the study of the transformation of phase I into phase II as a function of time at 298 K was made with a cylindrical CPS120 INEL (France) position sensitive detector consisting of 4096 channels and angular steps of about 0.03° (2Θ), and allowing for a powder diffraction pattern to be simultaneously recorded over a 2Θ range of 120°. The initial sample (phase II) was introduced in a Lindemann glass capillary of 0.5 mm diameter, annealed at 410 K for 0.5 h and quenched at 298 K at about 100 $K \cdot s^{-1}$. The capillary was immediately mounted on the goniometer circle of 250 mm radius of curvature, and was allowed to rotate around the Θ axis to ensure proper averaging over the crystallites. The time interval between successive patterns was 344 s, including 200 s for data collection. Result are shown in Fig. 3.

III. *p,T* DIAGRAM OF PIRACETAM

III.A. Equilibria Involving the Vapor Phase

III.A.1. Since the DSC measurements are performed in conditions (sealed pans with an inner dead volume) which allow the samples to evaporate until the dead volume is occupied by a saturating vapor, the transition temperatures are to be related to triple points involving a vapor phase, even when the vapor pressure is low enough for

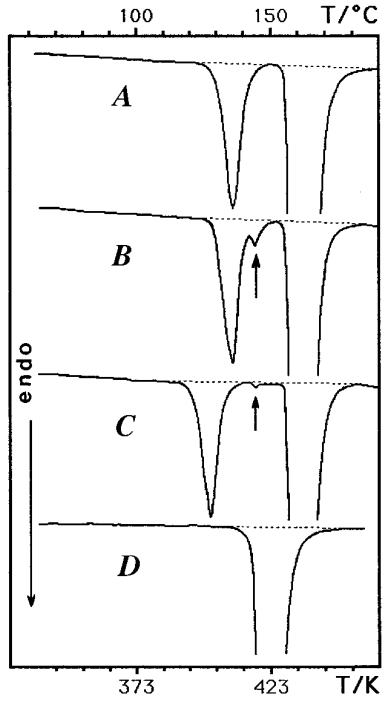

FIG. 2. DSC curves: (A, B) Phase II; (C, D) Phase III. Heating rate: 10 $K \cdot min^{-1}$.

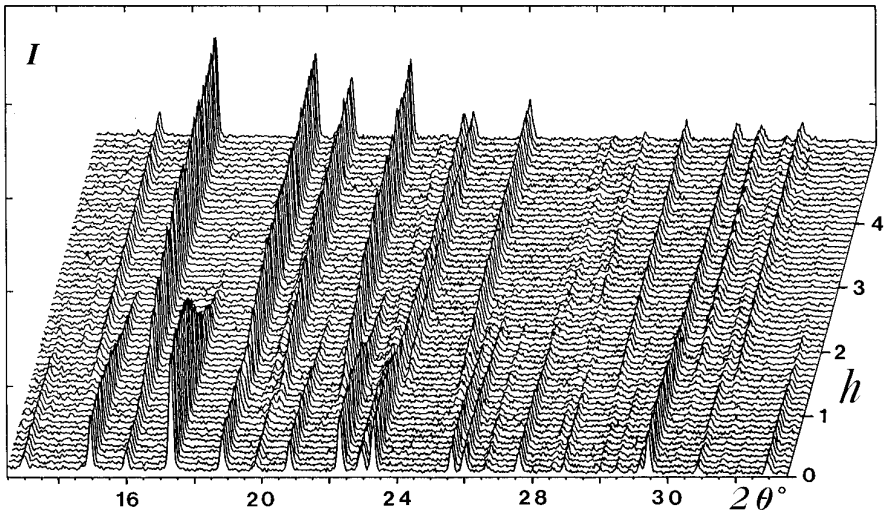

FIG. 3. Transformation of phase I into phase II at 298 K. Intensity I (arbitrary unit) vs Bragg angle ($2\theta°$), oblique axis: time (h).

partial sublimation (or boiling) of the condensed phases to be negligible.

In the case of Piracetam, the experiments described above provide us with information on some triple points involving the liquid (l) and the vapor (v) phases. Triple points (I–III–v), (I–II–v), (III–l–v), and (I–l–v) are located in the p,T diagram on the (I–v) and (l–v) curves at the temperatures of the (I–III), (I–II), (III–l), and (I–l) transitions, respectively, as shown in Fig. 4.

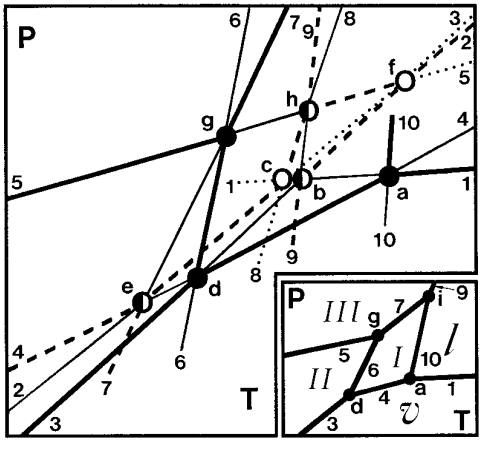

FIG. 4. Toplogical p,T diagram. Triple points: a^+ = I–l–v, b = II–l–v, c^+ = III–l–v, d^+ = I–II–v, e^+ = I–III–v, f = II–III–v, g = I–II–III, h = II–III–l, i = I–III–l, j* = I–II–l. (+: experimental, *: not represented). Two-phase equilibrium curves: 1 = l–v, 2 = III–v, 3 = II–v, 4 = I–v, 5 = II–III, 6 = I–II, 7 = I–III, 8 = III–l, 9 = II–l, 10 = I–l. Stability hierarchy. Triple points: black = stable, black and white = metastable, white = supermetastable. Two-phase equilibrium curves: thick = stable, thin = metastable, dashed = supermetastable, dotted = hypermetastable. Insert: stable phase regions whether curves 7 and 10 meet point i at high pressure.

Assuming that (I–l–v) is a stable triple point because it is the higher melting point (3), it may be inferred that (I–II–v) is also a stable triple point. Triple point (I–III–v) is then metastable.

III.A.2. The temperature of triple point (II–l–v), i.e., phase II melting point, can be determined as follows. By neglecting the specific heats of the differents forms, $\Delta_{fus}H(II)$, calculated by adding $\Delta_{(II\to I)}H$ to $\Delta_{fus}H(I)$, is equal to $+204\ J\cdot g^{-1}$ [$+201.7\ J\cdot g^{-1}$ in Ref. (13)]. Assuming a linear relationship between $\Delta_{fus}H(i)$ and $T_{fus}(i)$, $T_{fus}(II)$ is found at 415 K. This temperature is that of the weak endotherm recorded on some DSC curves (arrows in Figs. 2C and 2D). It can be related to some traces of phase II among phase III, as shown by XRD, or to an incomplete transition into phase I when heating phase III. In the first case, it corresponds to the melting of phase II traces, and in the second case, to the melting of residual phase III.

III.A.3. For further information on the p,T diagram, it has to be determined in which temperature range (low or high) the (II–v) and (III–v) curves intercept. In the first case, the (II–III–v) triple point would be at low temperature and phase III would be stable at temperatures lower than $T_{(II-III-v)}$. In the second case, triple point (II–III–v) would be metastable, and no stable phase region would be expected for phase III, except perhaps under high pressure.

Since the vapor pressures of the three forms are very low, the (I–v), (II–v), and (III–v) sublimation curves may be considered as straight lines. Assuming that the vapor pressure at triple point (I–III–v) is not significantly different from that at triple point (I–II–v), and assuming that it is the same for triple point (II–l–v) and (III–l–v), it may be observed in Fig. 4 that the difference between the temperatures of the experimental triple points involving

phases II and III decreases as temperature increases ($\Delta T = 7°$ at 396.5 K, and 3° at 414.5 K). Linear extrapolation results in $\Delta T = 0$ at 428 K, which has to be considered as the lowest possible temperature for triple point (II–III–v).

III.A.4. These results allow the equilibria involving the vapor phase to be drawn in the p,T diagram of Fig. 4. It is worth noting that, although arbitrary scales were used, the stability hierarchy can be deduced at any temperature from the relative positions of the sublimation curves by deducing the subsequent inequalities of the vapor pressures of each phase. It is read on the graph that (i) for $T < 392$ K, $p(\mathrm{II}) < p(\mathrm{III}) < p(\mathrm{I})$, (ii) for $392 < T < 399$ K, $p(\mathrm{II}) < p(\mathrm{I}) < p(\mathrm{III})$, and (iii) for $399 < T < 426$ K, $p(\mathrm{I}) < p(\mathrm{II}) < p(\mathrm{III})$.

III.B. Equilibria Involving Only Solid Phases

Using crystallographic and thermodynamic data found in the literature and those presented here, the slopes dP/dT of the three solid–solid equilibrium curves can be calculated with the Clapeyron equation. These curves, which intercept at triple point (I–II–III), are the boundaries of the stability domains of each phase as a function of pressure and temperature.

The molecular volumes of phases II and III (Table 1) are taken from Ref. (10) because the lattice parameter values have been obtained with the same apparatus, and refined by using a great number of reflections (about 100).

III.B.1. I–II and I–III equilibrium curves. Both transitions are endothermal on heating, and accompanied with positive volume changes (Table 1). Taking $T = 399$ K, $(dp/dT)_{(\mathrm{II}\to\mathrm{I})}$ is calculated at $+2.16\ \mathrm{MPa}\cdot\mathrm{K}^{-1}$, and with $T = 392$ K, $(dp/dT)_{(\mathrm{III}\to\mathrm{I})}$ is found at $+2.10\ \mathrm{MPa}\cdot\mathrm{K}^{-1}$.

III.B.2. II–III equilibrium curve. Although this transition is not observed, its enthalpy increment can be calculated as $\Delta_{(\mathrm{III}\to\mathrm{II})}H = +4\ \mathrm{J}\cdot\mathrm{g}^{-1}$ with the $\Delta_{(\mathrm{III}\to\mathrm{I})}H$ and $\Delta_{(\mathrm{II}\to\mathrm{I})}H$ values estimated at 395 K, i.e., the average value of the temperatures at which they have been observed. This agrees with the values from Ref. (13). This transition is accompanied with a positive volume variation. With $T = 395$ K, $(dp/dT)_{(\mathrm{III}\to\mathrm{II})}$ is found at $+1.66\ \mathrm{MPa}\cdot\mathrm{K}^{-1}$.

III.B.3. I–II–III triple point. This point may be positioned either on the stable part (at high pressure) or on the metastable extension (at low pressure) of the I–II equilibrium line, to which also belongs the stable I–II–v triple point. It depends on the difference in the values of the slopes of the I–III and I–II equilibrium curves that have to cross at (I–II–III). Assuming that such curves are straight lines over a wide pressure range, they can be described by the equations $p_{(\mathrm{III}\to\mathrm{I})}/\mathrm{MPa} = 2.10\ (T - 392)/\mathrm{K}$ and $p_{(\mathrm{II}\to\mathrm{I})}/\mathrm{MPa} = 2.16\ (T - 399)/\mathrm{K}$, respectively. The coordinates of triple point (I–II–III) are then $T = 662$ K and $p = 568$ MPa. Therefore, it is situated on the stable part of the I–II equilibrium line.

In order to keep points f, g, and h inside Fig. 4, the representation has been contracted so that the P values for these points appear as unrealistically low. This is also true for the corresponding T values (for instance $T\mathrm{a} < T\mathrm{g}$). This allows points e, d, c, b, and a to be positioned at their thermodynamical T values.

III.B.4. Discussion. Mainly because of the uncertainties of the ΔH measurements, small changes in the values of the slopes can drastically modify the description of the p,T diagram: if the calculated $\Delta_{(\mathrm{III}\to\mathrm{I})}H$ value ($\Delta_{\mathrm{fus}}H(\mathrm{III}) - \Delta_{\mathrm{fus}}H(\mathrm{I}) = +30\ \mathrm{J}\cdot\mathrm{g}^{-1}$) was used instead of the experimental one, the slope $(dp/dT)_{(\mathrm{III}\to\mathrm{I})}$ would be $+2.25\ \mathrm{MPa}\cdot\mathrm{K}^{-1}$. If the calculated ΔH value ($+6\ \mathrm{J}\cdot\mathrm{g}^{-1}$) for the transition II–III was used, the related slope would be $+2.49\ \mathrm{MPa}\cdot\mathrm{K}^{-1}$.

These results may be evaluated from the unambiguous relative positions of the (I–III–v), (I–II–v), and (II–III–v) triple points, that have to be crossed by curves 7 (I–III), 6 (I–II), and 5 (II–III) of Fig. 4, respectively.

—Hypothesis 1 (slope 5 > slope 7 > slope 6). Curves 7 and 6 cross at low pressure and low temperature. Triple point (I–II–III) is metastable because it is located on the metastable extension of curve 6. If slope 5 > slope 7, curve 5, which also crosses this triple point, cannot be directed toward triple point f (II–III–v) of Fig. 4, that has been proved to be positioned at high temperature. Therefore, slope 5 has to be lower than slope 6.

—Hypothesis 2 (slope 7 > slope 6 > slope 5). Curves 7 and 6 intercept as in hypothesis 1. Curve 5, which is the less positively slopped, can meet triple point (II–III–v). However, if it were true, phase III would have no stable phase region in the p,T diagram. Such a case has been described as "overall monotropy" (4), and it was shown how monotropy can be distinguished from high pressure enantiotropy. As phase III is the denser phase, it cannot be stabilized by a pressure decrease, as inferred by this hypothesis.

It may be concluded that slope 6 > slope 7 > slope 5. This agrees with what is found with the experimental values (enthalpies and densities) of Ref. (13), 2.26, 1.83, and 1.43 $\mathrm{MPa}\cdot\mathrm{K}^{-1}$, respectively.

III.B.5. II–III–l, I–III–l, and I–II–l triple points. Since volume changes at melting are not known, these triple points cannot be positioned from experimental data. Nevertheless, such volume changes, either positive or (seldom) negative, are mostly of ca. 5 to 10%. This allows the values of the slopes of the polymorph melting curves to be estimated between ±5 and ±13 $\mathrm{MPa}\cdot\mathrm{K}^{-1}$. Therefore, it may be assumed that these triple points, to which converge Si–Sj and Si–l curves, are located at high pressures. Stable parts of curves 7 and 10 meet at stable triple point i (I–

III–*l*) (Fig. 4 insert) together with the metastable part of curve 8. Curves 6 and 9 meet, at a pressure higher than that of point i, at metastable triple point I–II–*l*, which is also crossed by the metastable extension of curve 10. Triple point h (II–III–*l*) has to be located on curve II–III (curve 5 in Fig. 4), with which it shares two common phases. It can be noted that there are two parts with different metastability degrees on segment g–f, a metastable part from g and a supermetastable part from f. Such a change is indicative for the existence of triple point (II–III–*l*), at which curves II–*l* (9) and III–*l* (8) do cross.

IV. TIME-RESOLVED TRANSFORMATION OF PHASE I INTO PHASE II AT 298 K

The 3D plot in Fig. 3 shows that the I → II transformation spontaneously occurs within about 2 h at room temperature. For the transformation rate to be determined, the intensities of four strong reflections have been measured as a function of time: 021 and 002 for phase I and 002 and −112 for phase II. Fraction $x(t)$ of phase II at time t was determined by $x(t) = I(t)/I(\infty) = [I'_0 - I'(t)]/I'_0$, in which $I(t)$, for phase II, and $I'(t)$, for phase I, are intensities at time t, and $I(\infty)$ and I'_0 are the intensities for pure phases II and I, respectively. $x(t)$ values obtained from $I(t)$ closely agree with those independently obtained from $I'(t)$. This is indicative for a good randomization of the crystallite orientations in the capillary sample-holder, thus allowing further analysis of the transformation. For randomly oriented crystallites, isothermal transformations with time-dependent nucleation frequencies can be approximately described (14, 15) by the equation $x(t) = 1 - \exp(Kt^n)$, where K and n are time-dependent constants. When the nucleation frequency decreases as time increases, n values are generally found between 3 and 4 (15), as it is for the transformation I → II: the observed $x(t)$ values from the 4 sets of intensities satisfactorily fit the linear form $\ln[-\ln(1 - x(t)] = n \cdot \ln t + \ln K$ of the equation, with $\ln K = -16.341$ and $n = 3.4118$ ($r = 0.962$).

V. LATTICE-ENERGY CALCULATIONS AND CONFORMATIONS COMPARISON

V.A.

By using the atom–atom potential method (16) with potentials from Ref. (17) and atom charges calculated by the CNDO/2 method, lattice energies have been found (12) at −87.29, −97.30, and −99.44 kJ · mol^{-1} for phases I, III, and II, respectively. These values indicate that phase II is stabler than phase III, which is in turn stabler than phase I. However, this stability hierarchy does not take pressure and temperature effects into account, although it is the same as that obtained from the relative positions of the sublimation curves at room temperature in the p,T diagram. This agreement between both approaches may be due to the fact that sublimation curves do not cross at lower temperatures, thus leading to the same inequalities at 0 K as those from lattice energy calculations.

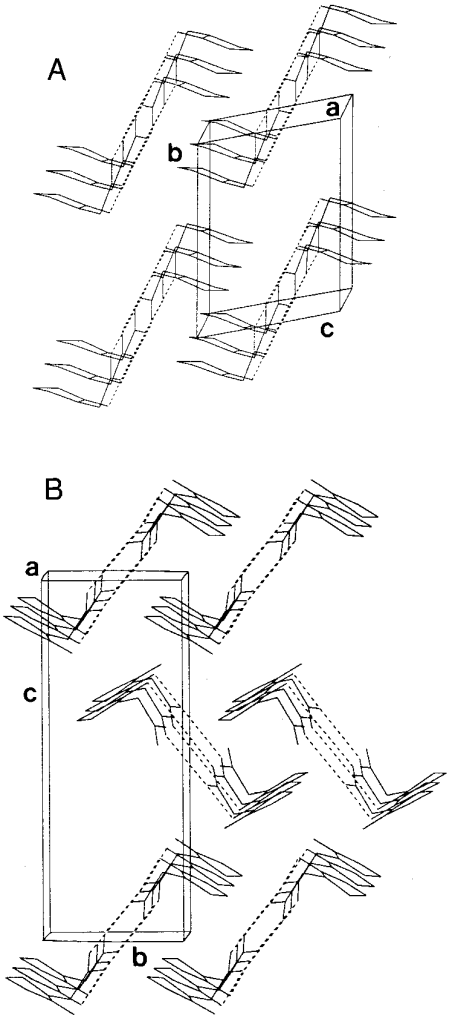

FIG. 5. Molecular packings. (A) Phase II. Hydrogen-bonded dimers are stacked along direction *a* in parallel chains; (B) Phase III. Similar chains are stacked along *a*. Note the herringbone-like projection of the dimers onto plane *bc*.

V.B.

Comparison of the crystal packings in these phases has been briefly presented elsewhere (12), and the graph-set method (18, 19) was used in order to describe the hydrogen-bonds patterns in these polymorphs. The main structural features are as follows: (i) phases II and III consist of similar networks (Figs. 5A and 5B) made of centrosymmetrical hydrogen-bonded dimers of Piracetam molecules (Fig. 6A), as usually found in primary amide crystals (20). (ii) In phase I, cyclic dimers are no longer observed (Fig.

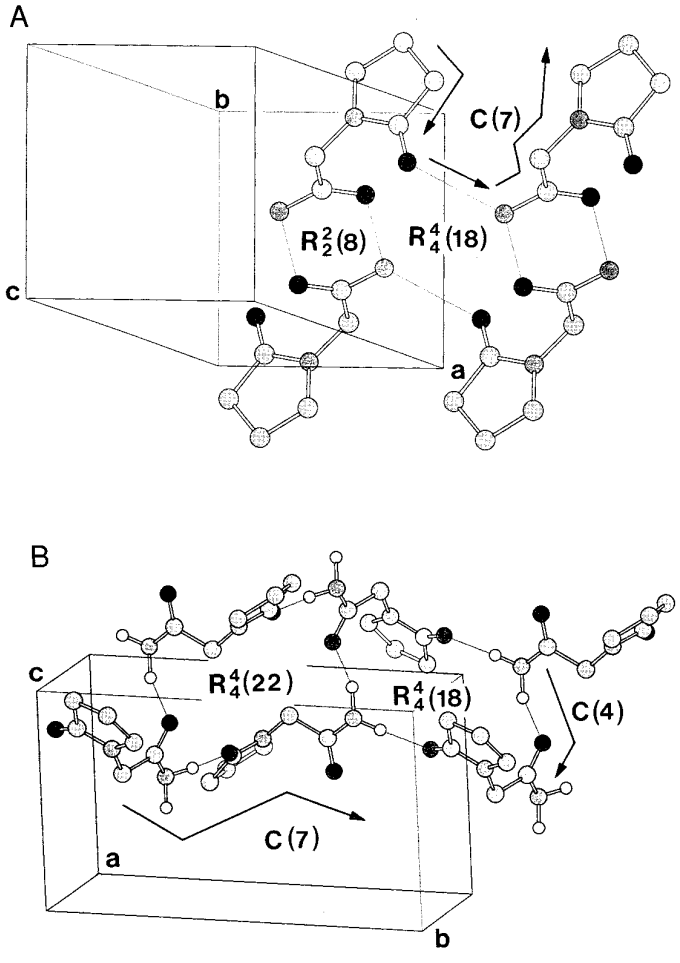

FIG. 6. Graph-set analysis (H-atoms omitted for clarity). (A) Phase II and phase III (here drawn); (B) Phase I. Graph-set, $G_d^a(r)$, specified using the pattern designator G, its degree r (number of atoms, including H atoms, in a ring or in the repeat length in a chain), and the numbers d and a of donors and acceptors, respectively. $G = C$ (infinite chain), D (definite chain), R (ring), or S (intramolecular ring). After the graph-sets assignment, the total hydrogen-bond network (primary (N_1) + secondary (N_2) networks) is stated as a series of graph-sets (Phases II and III: N_1 = C(7) $R_2^2(8)$, $N_2 = R_4^4(18)$; phase I: N_1 = C(4) C(7), $N_2 = R_4^4(18)$ $R_4^4(22)$).

6B). Two types of hydrogen bonds link the molecules in two types of perpendicular infinite chains, that form a two-dimensional network. (iii) Four hydrogen bonds per molecule are found in each structure.

V.C.

Two torsional angles, φ and ω, may vary in the molecule (Fig. 7A) because of rotational freedom around C5–N1 and C5–C6 bonds. A conformational energy map (Fig. 7B), calculated by means of semi-empirical AM1 calculations (21) using the Mopac program (22), agrees with the map calculated *ab initio* (6): the energy minimum is found for $\varphi = 74°$ and $\omega = 298°$. It can be seen how the crystal packings contribute to the stabilization of conformations with energies higher than that of the isolated molecule. In the crystal structures, φ is increased by ca. 25° and ω is decreased by ca. 130°. Similar conformations are found in the crystal structures of phases II and III, and the lower conformational energy is found in phase I. It may be concluded that the less stable conformation is preferred at room temperature, at which phases II and III are stabler

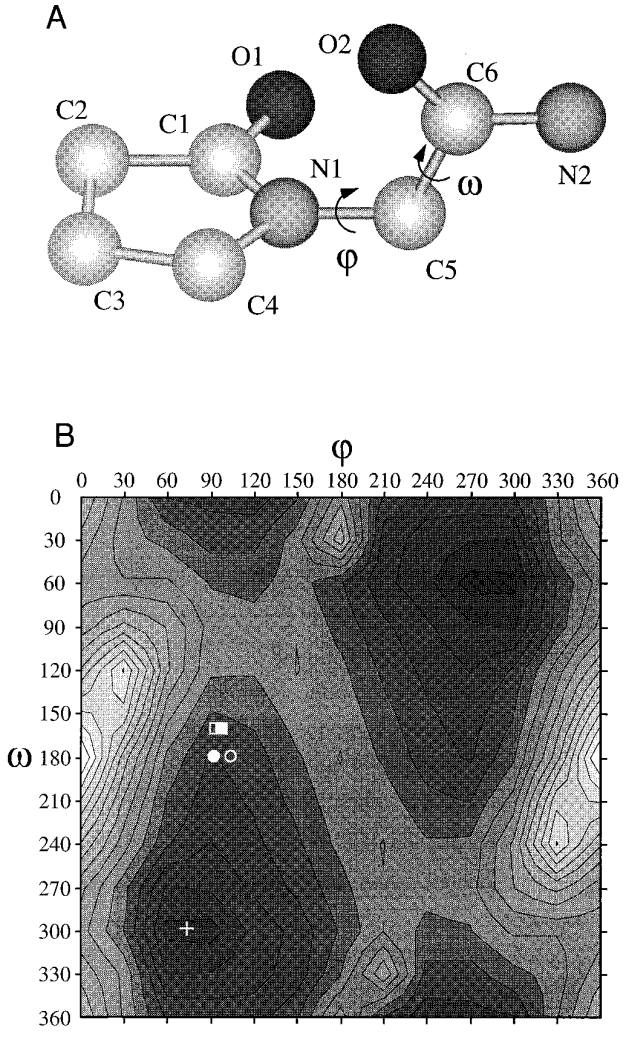

FIG. 7. (A) Atom numbering (H atoms omitted); (B) Energy contour map of the isolated molecule versus torsional angles $\varphi°$ (C6–C5–N1–C1) and $\omega°$ (N1–C5–C6–N2). Energy minima: white cross denotes an isolated molecule; empty (X-rays) and full (AM1) squares denote phases II and III, respectively; empty (X-rays) and full (AM1) circles denote phase I. Contours of equal energy are drawn with an increment of 3.50 kJ from the lowest energy level (dark-grey: -338.58 kJ · mol^{-1}) to the highest one (white: -286.08 kJ · mol^{-1}). For the AM1 calculations in the crystal structures, ω values have been fixed at 159.25° (phases II and III) and 178.39° (phase I). If not fixed, ω free rotation would result in an intramolecular O1 · · · H–N2 hydrogen bond not observed experimentally.

than phase I. So dimerization may contribute to stabilize the packings in phases II and III. The heat of formation of a hydrogen-bonded dimer (−687 kJ per dimer) is found, by AM1 calculations, lower than that of two monomers (−327 kJ per monomer) by −34 kJ, i.e., −17 kJ per hydrogen bond, in agreement with *ab initio* calculations (6). It also has to be noted that the less dense packing of phase II is spontaneously preferred to that of phase III at room temperature, which is not usual.

VI. CONCLUDING REMARKS

DSC measurements on crystallographically defined phases and density values from crystal structure parameters allowed us to draw a topological p,T state diagram of Piracetam. The stability hierarchy of its polymorphs at any temperature may be obtained from vapor pressure inequalities. At 298 K the hierarchy is the same as that obtained from lattice-energy calculations. It also agrees with the transformation of phase I into phase II spontaneously occuring within a few hours at 298 K, but it disagrees with the stability hierarchy deduced from the energy vs temperature diagram in Ref. (13). The source of this disagreement is the temperature of transitions I–II and I–III. If $T_{III \to I}$ was higher than $T_{II \to I}$, as claimed in Ref. (13), the topological p,T diagram would be like that in Fig. 8. Triple point e (I–III–v) would be stable and triple point d (I–II–v) would be metastable. It follows that triple point f (II–III–v) would be also metastable and located at the crossing point of curves 3 (II–v) and 2 (III–v), i.e., between triple points e and c (III–l–v). Now taking into account inequalities between the slopes dp/dT of the I–II, I–III, and II–III equilibrium curves (same result from both studies), it comes that triple point g (I–II–III) would be metastable and located either at point g_1 or at point g_2, or even at point g_3, where I–II and II–III, I–II and I–III, and I–III and II–III lines cross, respectively. There are also two possible settings for curve 5. Whichever the choice, it does not lead to a unique triple point (I–II–III). If, for instance, point g_3 or point g_1 are considered, phase II would be stable under pressure, as shown in Fig. 8, insets A and B, respectively. Such hypotheses, which disagree with the density hierarchy of phases II and III, need slope 6 (I–II) to be lower than slope 7 (I–III) (inset A) or even slope 7 to be negative (inset B). If point g_2 is considered (Fig. 8, inset C) no stable region for phase II can be found although the relative positions of slopes 5, 6, and 7 are the same as in Fig. 4. Therefore, phase II behavior would be monotropic (4). Such an outcome disagrees with the enantiotropic behavior of phase II, which is also found in Ref. (13).

In this paper, it is shown that phase III has to be considered as a high-pressure phase. Furthermore, lattice-energy calculations surprisingly led to a fourth possible crystal structure with a lattice energy as low as $-100.78\ \text{kJ} \cdot \text{mol}^{-1}$ (12), which has not been experimentally isolated yet. As this hypothetical phase is unlikely to account for the structure of any metastable phase among those transitorily observed (13), low-temperature experiments would be of interest to check whether this phase really exists.

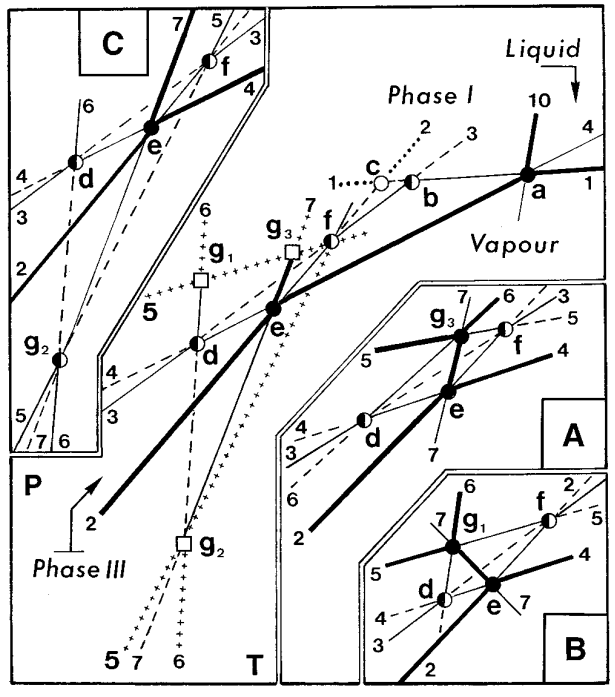

FIG. 8. Piracetam p,T diagram constructed from data in Ref. (13). ($T_{fus}(I) > T_{fus}(II) > T_{fus}(III)$, $T_{II \to I} > T_{III \to I}$, and $dp/dT_{(I-II)} > dp/dT_{(I-III)} > dP/dT_{(II-III)}$). Stabilities, triple points, and two-phase equilibrium curves with same labelling as in Fig. 4. g_1, g_2, and g_3 are possible locations of triple point g (I–II–III). +++ denotes extensions of the two-phase equilibrium curves for which stability hierarchies are not taken into account.

It is also worth noting that Piracetam is a another example of polymorphism according to which the more stable conformation can be observed in the less stable lattice at room temperature, as previously stated (23, 24).

ACKNOWLEDGMENT

We acknowledge Dr. F. Lambert, Isochem (F-92230 Gennevilliers), who kindly supplied us with Piracetam samples.

REFERENCES

1. S. R. Byrn, "Solid-State Chemistry of Drugs." Academic Press, New York, 1982.
2. W. Ostwald, *Z. Physikal. Chem.* **22,** 289 (1897).
3. R. Céolin, S. Toscani, V. Agafonov, and J. Dugué, *J. Solid State Chem.* **98,** 366 (1992).
4. R. Céolin, S. Toscani, and J. Dugué. *J. Solid State Chem.* **102,** 465 (1993).

5. S. Toscani, A. Dzyabchenko, V. Agafonov, J. Dugué, and R. Céolin, *Pharm. Res.* in press.
6. G. Bandoli, D. A. Clemente, A. Grassi, and G. C. Pappalardo, *Mol. Pharmacol.* **20**(3), 558 (1981).
7. A. Weltscheva Pavlova, *Pharmazie* **34** (17), 449 (1979).
8. A. Pavlova, N. Konstantinova, H. Dashkalov, and A. Georgiev, *Pharmazie* **38**(9), 634 (1983).
9. A. V. Pavlova, *Pharmazie* **39**(4), 272 (1984).
10. G. Admiraal, J. C. Eikelenboom, and A. Vos, *Acta Crystallogr. Sect. B* **38,** 2600 (1982).
11. Z. Galdecki and M. L. Glowka, *Pol. J. Chem.* **57,** 1307 (1983).
12. D. Louër, M. Louër, V. A. Dzyabchenko, V. Agafonov, and R. Céolin, *Acta Crystallogr. Sect. B* **51,** 182 (1995).
13. M. Kühnert-Brandstätter, A. Bürger, and R. Völlenklee, *Sci. Pharm.* **62,** 307 (1994).
14. Melvin Avrami, *J. Chem. Phys.* **7,** 1103 (1939); *J. Chem. Phys.* **8,** 212 (1940); *J. Chem. Phys.* **9,** 177 (1941).
15. D. Turnbull, *in* ''Solid State Physics'' (F. Seitz and D. Turnbull, Eds.), Vol. 3, p. 252. Academic Press, New York, 1956.
16. A. J. Pertsin and A. I. Kitaigorodskii, ''The Atom–Atom Potential Method.'' Springer-Verlag, New York, 1987.
17. F. A. Momany, L. M. Carruthers, R. F. McGuire, and H. A. Scheraga, *J. Phys. Chem.* **78,** 1595 (1974).
18. M. C. Etter, *Acc. Chem. Res.* **23,** 120 (1990).
19. M. C. Etter, J. C. MacDonald, and J. Bernstein, *Acta Crystallogr. Sect. B: Struct. Sci.* **46,** 256 (1990).
20. A. T. Hagler and L. Leiserowitz, *J. Am. Chem. Soc.* **100,** 5879 (1978).
21. M. J. S. Dewar, E. G. Zoebisch, E. F. Healy, and J. J. P. Stewart, *J. Am. Chem. Soc.* **107,** 3902 (1985).
22. J. J. P. Stewart, *J. Comput.-Aided Mol. Des.* **4,** 1 (1990).
23. J. Caillet, P. Claverie, and B. Pullman, *Acta Crystallogr. Sec. B Struct. Crystallogr. Cryst. Chem.* **32,** 2740 (1976).
24. J. Bernstein and A. T. Hagler, *J. Am. Chem. Soc.* **100,** 673 (1978).